ISSN 1392–1320 MATERIALS SCIENCE (MEDŽIAGOTYRA). Vol. 25, No. 3. 2019

Defects Promoted Topotactic Transformation from $Co(OH)_2$ Nanodiscs to Co_3O_4 Nano Octahedra

Fei HUI [1], Chunhui WANG [1], Yanhui CHEN [1]*, Junfeng ZHOU [2], Pierce MAGUIRE [2], Hongzhou ZHANG [2]

[1] *Institute of Microstructure and Properties of Advanced Materials, Beijing University of Technology, Beijing, 100124, P. R. China*
[2] *School of Physics and Centre for Research on Adaptive Nanostructures and Nanodevices (CRANN), Trinity College Dublin, Dublin 2, Republic of Ireland*

crossref http://dx.doi.org/10.5755/j01.ms.25.3.22005

Received 05 November 2018; accepted 06January 2019

Topotactic transformation was one of the most frequently related processes in the synthesis process of cobalt oxide nanomaterials. Microstructural evolution studies of this process inform and enable the process of controlling the shape of the final products. One such topotactic transformation was investigated here, the transition from $Co(OH)_2$ hexagonal nano platelets to Co_3O_4 octahedra by a hydrothermal method in an ammonia solution. Evolution of phase and microstructure was studied during different stages of the reaction to reveal the criteria which prompt this transformation. A phase transformation from $Co(OH)_2$ to CoOOH and hence to Co_3O_4 was observed. High resolution transmission electron microscopy and image simulation were utilised to disclose the role of defects in the topotactic transformation. A high density of defects including edge dislocations and displacements was found on the surface of dried $Co(OH)_2$ nano platelets. The coexistence of CoOOH domains embedded in the $Co(OH)_2$ surface indicates the absence of the hydrogen bonds of the starting materials. The breaking of hydrogen bonds leads to bonding variation and the further creation of defects, finally prompting the transformation from $Co(OH)_2$ to CoOOH. The breaking of hexagonally arranged hydrogen bonds creates seeds for the formation of Co_3O_4.

Keywords: topotactic transformation, defects, CoOOH domains, Co_3O_4 octahedrons, $Co(OH)_2$ platelet.

1. INTRODUCTION

Topotactic transformation refers to the phase transition between two crystalline materials that have definite and reproducible crystallographic relationships. The transformation is responsible for the formation of some metal oxides, which are obtained from thermal dehydrations of corresponding hydrates [1, 2]. For a typical example, topotactic transformation occurs between FeOOH and Fe_2O_3, in which dehydration and atomic rearrangement are involved according to their intrinsic structural relationship [3, 4]. Recently, topotactic transformation has also been used for the synthesis of metal oxide nanomaterials from the corresponding metal hydroxide. Spinel structure Co_3O_4 is the typical material synthesized by topotactic transformation in the case of thermal treatment applied to its corresponding $Co(OH)_2$ [2]. Porous, structured Co_3O_4 has been fabricated using topotactic synthesis with $Co(OH)_2$ nanoflakes as precursors and has been described as a promising material for lithium-ion batteries [5]. Furthermore, topotactic transformation can be used for shape control in the synthesis of needle-like Co_3O_4 nanotubes [6], nanoboxes [7], nanotubes [8] and nanobelts [5, 9].

Hexagonal β-$Co(OH)_2$ has a brucite-like layered structure with a relatively large interlayer spacing of 0.47 nm while Co_3O_4 has a face-centred close-packed cubic structure with a Co-O octahedron in it. Topotactic formation from $Co(OH)_2$ into Co_3O_4 includes diffusion of Co^{3+} into the interlayer space and oxidation of half of the Co^{2+} in the brucite-like sheets of β-$Co(OH)_2$. The transformation involved can be described simply by the well-known thermodynamically favourable oxidation reaction: $Co(OH)_2+O_2 \rightarrow Co_3O_4$, or can be considered from a crystallographic perspective as the diffusion of Co atoms into interlayer space to form a Kagome net arrangement. However, microstructural studies of topotactic transformation between $Co(OH)_2$ and Co_3O_4 to date have mainly focused on atomic illustration/simulation of sites or the variation of elements. Some experimental work has briefly mentioned structural and valence evolution during the transformation process. Yeh's heating experiments under 500 °C – 800 °C indicate that the formation of porous plate-like Co_3O_4 structures by thermal treating $Co(OH)_2$ platelets was related to the surface defects of precursors [9]. Some of the literature has mentioned large quantities of dislocations on the surface of the original $Co(OH)_2$ or heat treated Co_3O_4 platelet. It is strongly suggested that these defects play an important role in the phase and structural transformation [10]. Further understanding of the structural and valence evolution still needs to be established. Limited work using high resolution transmission electron microscopy (HRTEM) [11] focused on defects in the $Co(OH)_2$ and their role in structural transformation. However, precise atomic scale microstructural information could lead to a detailed understanding of the effect of these defects on topotactic

* Corresponding author. Tel.: +86-10-67396521; fax: +86-10-67396521.
E-mail address: *yhchen@bjut.edu.cn* (Y. Chen)

transformation in the Co_3O_4 system. It is noted that products after topotactic transformation usually possess a uniform size and shape, which contributes significantly to broadening their applications [9, 12 – 14].

In this paper, an investigation was performed of the topotactic transformation from $Co(OH)_2$ nano platelets to octahedral Co_3O_4 nanoparticles by hydrothermal method in an ammonia solution. Microstructural and phase evolution were studied during different stages of the reaction to disclose the dominant factors which prompt this transformation. HRTEM and related simulations, electron diffraction (ED) and electron energy loss spectroscopy (EELS) will be carried out to disclose the microstructure and bonding variation between the starting material $Co(OH)_2$, the intermediate CoOOH, and the final octahedral Co_3O_4. An atomic model will also be illustrated to explain the transformation mechanism.

2. EXPERIMENTAL

The synthesis procedure included two hydrothermal steps, which include the preparation of $Co(OH)_2$ nanoplate-like starting material and the final Co_3O_4 nanoparticles respectively. In the first step, 0.002 mol $CoCl_2 \cdot 6H_2O$ was dissolved in 20 mL deionized water. 20 mL of a 0.5 M NaOH solution was then added to the reaction mixture during stirring. Further 5 minutes was then stirred and the solution was heated at a temperature of 120 °C for 6 hours in a Teflon autoclave. The autoclave was cooled down to room temperature after reaction. The collected brown gel-like precipitate from the bottom of the autoclave was then washed with distilled water and ethanol. The precipitate was dried in an oven at 80 °C for 24 hours and a homogeneous dark brown powder was finally obtained. This powder was used as the original material for topotactic transformation reaction study. In the following process, 0.02 g of the powder was dispersed in a 40 mL of an aqueous ammonia solution (2.5 wt.%). The mixture was then put into a Teflon steel of 50 ml autoclave and heated to 120 °C from 30 minutes to 6 hours respectively. A black powder was obtained after reaction and it was filtered off and washed many time with deionised water and ethanol to keep the sample clean enough for characterization.

An X-ray diffractometer (XRD) of BRUKER-D8 ADVANCE diffractometer was used with graphite monochromatized Cu Kα radiation flux and the scanning rate is 0.02^o s^{-1} with a 2θ range of 10 – 90°. Scanning electron microscope (SEM) of Carl Zeiss Ultra was used to image the morphologies. The samples were then dropped cast from solution on an amorphous carbon film and dried in air for the transmission electron microscopy (TEM) characterization. A 300 kV FEI Titan TEM capable of performing electron energy loss spectrum (EELS) were used for these experiments. A large amount of individual nanoparticles was characterized to determine representative structures and morphologies in all cases. Atomic model and high resolution image simulations were carried out on Crystalmaker and JEMS software packages.

3. RESULTS AND DISCUSSION

Fig. 1 gives the crystal structures of typical products characterized by XRD. The XRD pattern in Fig. 1 a gives the starting material (precursors or after reaction of 0 min) that contains two phases: the dominant phase is trigonal β-$Co(OH)_2$ phase indexed with black squares symbols (JCPDS 30-0443), while minor phase is rhombohedral CoOOH phase (JCPDS 73-1213) as indexed blue triangular symbols. A typical TEM image, as shown in the right of XRD pattern in Fig. 1, give typical morphologies of the starting $Co(OH)_2$ nanoplate. The largest facet of the plate-like particle is its close-packed [15] plane of trigonal β-$Co(OH)_2$ as shown TEM image and XRD pattern. The dominant phase was then transferred to rhombohedral CoOOH phase after reaction for 30 minutes as shown in Fig. 1 b and some residual $Co(OH)_2$ phase (black square symbol indexed). The morphologies in TEM images show that the products now become a mixture of plate-like and rhombohedral particles. All products changed to the spinel Co_3O_4 phase (JCPDS 42-1467) after a reaction for 6 hours (Fig. 1 c) in ammonia solution by XRD pattern and TEM image in Fig. 1. The oxidation follows a process from $Co(OH)_2$ nanoplates to CoOOH then to octahedral Co_3O_4 particles at reaction temperature of 120 °C.

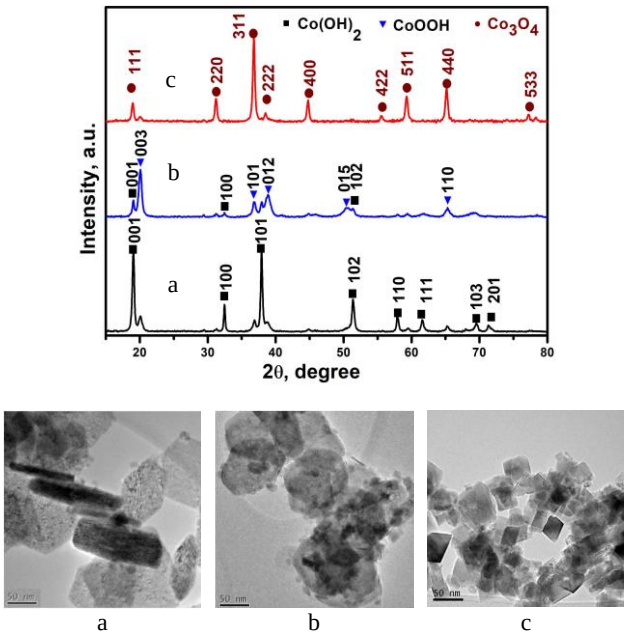

Fig. 1. XRD patterns and its corresponding TEM images: a – starting material $Co(OH)_2$ nanoplates; b – reaction after 30 min; c – reaction after 6 h

It was also noted that if we use as-grown nanoplates as the precursors, the yield of octahedra is very low (about 10 % from SEM image statistics). So it is necessary to compare morphological and valence differences between as-grown and dried nanoplate precursors. Fig. 2 gives the morphological and EELS spectra of as-grown and dried nanoplates. From Fig. 2, we can see as-grown samples are made of perfect nanoplates about 100 – 150 nm with a smooth border and a trace of nanoparticles (less than 2 % in quantity). After drying, it can be seen that the diameters of the nanoplates decrease and a rough border appears accompanied with more small nanoparticles (about 10 % in quantity). TEM images in Fig. 2 c and d give similar results to the SEM images. However, the diffraction

pattern in the inset of the TEM images shows sharper and clearer diffraction rings in dried samples than in as-grown samples. It indicates an increase in the crystallisation of the structure after drying. EELS spectra of O-K and Co-L edges of these two samples in Fig. 2 e and f indicate that a pre-peak in the O-K edge appears in the dried sample while it is nearly invisible in as-grown sample. As it is known that this pre-peak exhibits the appearance of trivalent cobalt in a sample, this means that the $Co(OH)_2$ (or part of) has been oxidized to CoOOH after the drying process. This oxidation process can also be seen in the Co-L edge as the integration area of L_3/L_2 increases in the sample after drying. In Fig. 2 f, we initialize the L_3 peak, so the height increase of L_2 peak indicates an increase in the ratio of Co^{3+} after drying compared to as-grown samples.

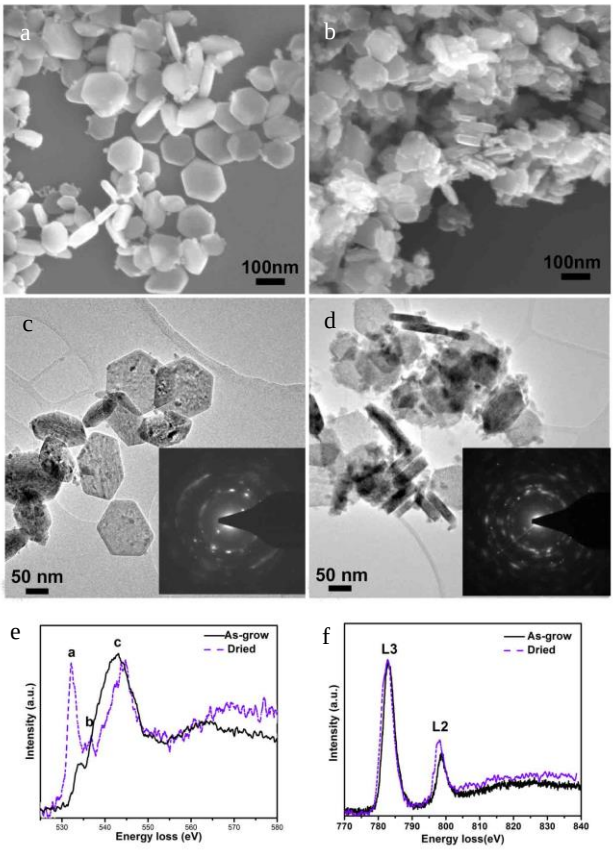

Fig. 2. SEM and TEM images and EELS spectra of a, c, e – as-grown samples; b, d, f – dried samples

A TEM image and its corresponding dark field image on specified diffraction spot can give the phase distribution in a multiphase system. Fig. 3 give the dried sample and corresponding dark field image by choosing CoOOH [110] diffraction spot and it indicates that CoOOH nanoparticles formed on surface after drying process especially on the borders of the plates.

HRTEM is a powerful technique to observe morphologies of nanomaterials and then to disclose the mechanism of shape transformation. Fig. 4 a – e are typical TEM and HRTEM images on plane-view and side-view of dried $Co(OH)_2$ nanoplates. Large quantity of distortions can be seen on a typical side-view (*a-c* plane) image as shown in Fig. 4 a. Two typical parts of the distortions in Fig. 4 a were enlarged and shown in Fig. 4 b and c. There was a translation about 0.65 Å from the left part to the right part in Fig. 4 b. Edge dislocation in Fig. 4 c can be regarded as an extra [110] plane in the left inserted into left part. Fig. 4 d shows one typical dislocation-filled nanoplate from top view (*a-b* plane), high concentration of dislocations connected to form a network structure.

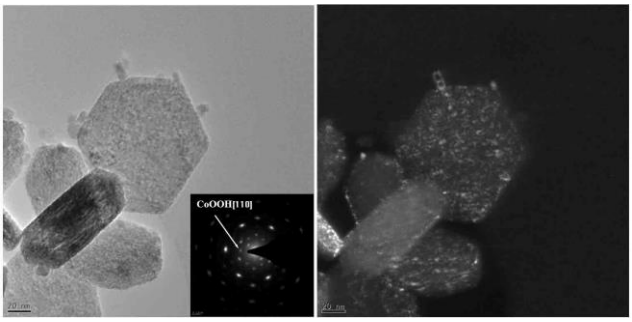

a b

Fig. 3. a – bright field image of dried sample and its diffraction pattern; b – dark field image by using CoOOH [110] diffraction spot

In the enlarged areas as shown in Fig. 4 e, one hexagonal convex can be distinguished due to the contrast it exhibits when compared with its background. The formation mechanism of this hexagonal convex-shaped structure will be discussed in the following part. A HRTEM simulation was also carried out to evaluate our conjecture as shown in Fig. 4 e. A slab was constructed by conjugating few layers of CoOOH (left part) and $Co(OH)_2$ (right part) together. HRTEM simulations in Fig. 4 e suggest an obvious difference between the $Co(OH)_2$ part and CoOOH part (thickness: 36.7 nm, defocus: –35 nm, accelerating voltage: 300 kv).

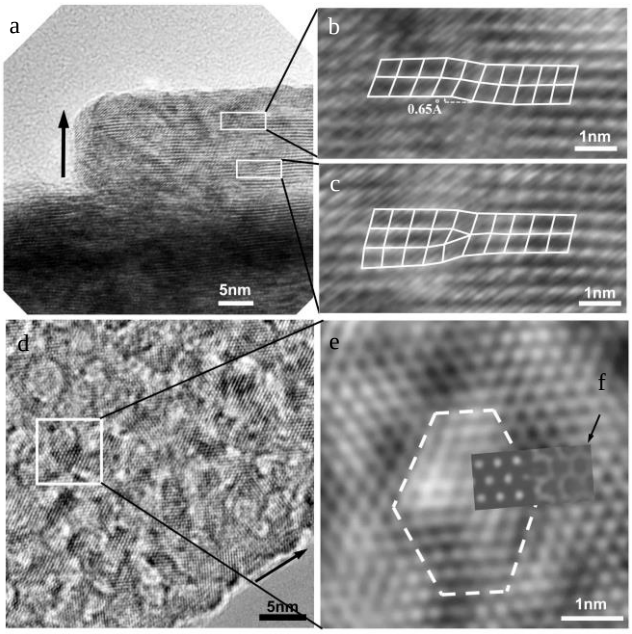

Fig. 4. a, b, c – TEM and HRTEM image of dried samples from side-view, two typical dislocations; d, e – top view, one hexagonal convex; f – HRTEM simulation from *a-c* plane. Simulation using JEMS software using multislice theory, defocus: –35 nm, thickness: 36.7 nm

The simulation was coincident with the experimental

images in squares as plotted across the boundary of bright hexagons embedded in dark contrast background in Fig. 4 e. Fig. 5 a and b give the bonding and atomic difference of nanodiscs of as-grown in solution and dried in air respectively. As-grown nanodiscs with $Co(OH)_2$ phase has a smooth surface with OH^- bonds exposed to the solution which contains lots of OH ligands as well. After drying in air, hydrogen atoms are lost in most sites and even some inner OH bonds broken to create some concave structure as shown in Fig. 5 b. A connection between $Co(OH)_2$ and CoOOH will be formed as shown in Fig. 5 c and d. Comparison from atomic structure of the two phases from *a-c* plane indicate that the distance between two layers of oxygens along c direction will shrink from 2.66 to 2.59 Å after oxidation. It means that the thickness will decrease slightly if $Co(OH)_2$ was oxidized to CoOOH by losing H atoms. Partial shrinkage in thickness will induce disorders between the shrinking and the original parts along the c-direction. A lot of translation and edge dislocations in the c-direction are thus created and connected to a dislocation network. However, seen from *a-c* plane as shown in Fig. 5 d, only H atoms are shown to simplify and illuminate the oxidation process in the left of the picture, and different layers of H were dyed in purple and pink colour. Large red balls represent O atoms, and small red balls represent Co atoms. In CoOOH only one layer of H atoms exist to form a centred hexagon, while two layers of centred hexagonal hydrogen atoms arrange crossly in $Co(OH)_2$. It means that if $Co(OH)_2$ loses one layer of hexagonal-arranged hydrogen atoms after oxidation to form CoOOH, then a hexagonal CoOOH particle is the most probable shape.

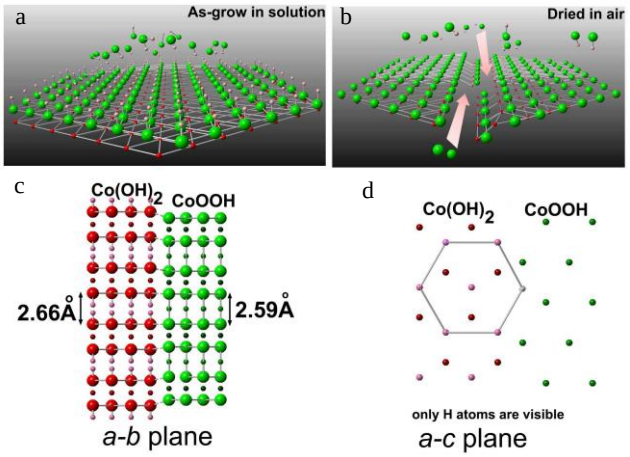

Fig. 5. Atomic model of: a – as-grown nanodiscs in solution; b – dried nanodiscs in air; c – atomic model of connection between $Co(OH)_2$ and CoOOH from a-b plane; d – a-c plane in which different colors and sized balls represent different atoms as indexed in images

Fig. 6 a shows a typical TEM image of coexisting Co_3O_4 and CoOOH using dried nanodiscs as precursors after reaction for 45 min in dilute solution at 120 °C. In the right part of the image, a platelet can be found while in the left part a hollow skeleton shaped plate is shown. This skeleton was made of nanoparticles of 30 – 60 nm. Some of this contains octahedron-like shape as shown in the top left which can be drawn in atomic model as in Fig. 6 b, which is near to Co_3O_4 {111} direction. The CoOOH platelet has a {001} direction face to us. We can conclude that the orientation relationship is as follows: $\{111\}_{Co3O4}//\{001\}_{CoOOH}$, it is means that close-packed faces of Co_3O_4 and CoOOH are nearly parallel.

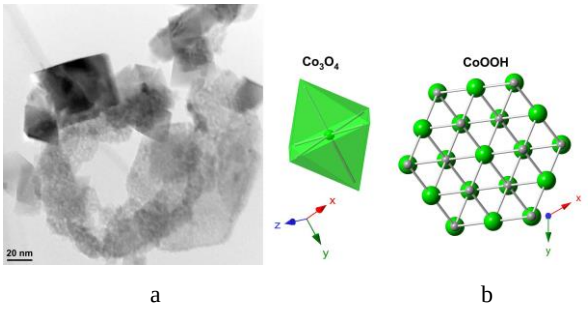

Fig. 6. a – TEM image demonstrating the coexistence of Co_3O_4 octahedra and CoOOH platelets; b – atomic orientation shown schematically

From above analysis, the topotactic transformation from β-$Co(OH)_2$ nano platelets to octahedral Co_3O_4 nanoparticles can be described as follows: after hydrothermal reaction, the as-grown plate-like nanoparticles are $Co(OH)_2$. The drying process causes $Co(OH)_2$ to lose several layers of hydrogen randomly. A lot of defects were thus created, causing the surface to become convex and concave as can be seen in TEM or HRTEM images in Fig. 4. Hydrogen atoms in $Co(OH)_2$ crystals were arranged as two alternating parallel layers of hexagons as illustrated in the atomic model in Fig. 5. Losing one layer of hydrogen atoms during the oxidation process will cause the formation of a hexagonal CoOOH border surrounding $Co(OH)_2$. This explains our observation of small hexagonal CoOOH regions embedded in $Co(OH)_2$ background (Fig. 4 e). These hexagonal CoOOH regions form seeds for the growth of Co_3O_4 in the hydrothermal oxidation process. There are many reports [6, 10] that oxidation of $Co(OH)_2$ platelets in the atmosphere can form porous Co_3O_4 platelets. However, there are no such reports of octahedral particles. Platelet $Co(OH)_2$ precursors in our experiments are placed in a high pressure and temperature environment with about 2 – 4 times standard atmosphere pressure. The surface potential of the plate will be higher than standard ball-like particles. Furthermore, many defects exist on the surface of a $Co(OH)_2$ plate which weaken the bonding between OH groups and act as an origin for breaking after continuous force in the autoclave. Co_3O_4 has a cubic spinel structure containing Co^{3+} in an octahedral coordination and Co^{2+} in a tetrahedral coordination, therefore Co_3O_4 has a tendency to grow into polyhedrons. Over a period of time, unstable CoOOH will transform to the stable FCC Co_3O_4 phase by adding one layer of Co atoms. The FCC structure of Co_3O_4 causes it to have expose as much as possible close-packed surface {111} planes hydrothermal water, then octahedron with largest {111} forms after long term of hydrothermal oxidation.

4. CONCLUSIONS

A topotactic transformation was demonstrated from $Co(OH)_2$ nano platelets to octahedral Co_3O_4 nanoparticles

by a hydrothermal method in an ammonia solution. Evolution of microstructure and phase was studied during different stages of the reaction to determine the principal reasons for this transformation. A phase transformation from $Co(OH)_2$ to CoOOH and then to Co_3O_4 was observed. A high density of defects including edge dislocations and displacements was found on the surface of dried $Co(OH)_2$ nano platelets. Imaging from a high resolution transmission electron microscope coupled with image simulation allowed the determination of the role of defects in the topotactic transformation. The breaking of uniformity in the weak hydrogen bond network induces bonding variation and the creation of further defects, finally prompting the transformation from $Co(OH)_2$ to CoOOH. The breaking of hexagonally arranged hydrogen bonds provides seeds for the formation of Co_3O_4.

Acknowledgments

This work was supported by National key research and development program No. 2016YFE0105700, Beijing Natural Science Foundation No.1182005, Natural Science Foundation of China in grants No. 51872008, 11404014, 51471008, 11327901 and the Importation and Development of High-Caliber Talents Project of Beijing Municipal Institutions (CIT&TCD201504013).

REFERENCES

1. **Wang, Z., Huang, B., Dai, Y., Zhu, X., Liu, Y., Zhang, X., Qin, X.** The Roles of Growth Conditions on The Topotactic Transformation from $TiOF_2$ Nanocubes to 3D Hierarchical TiO_2 Nanoboxes *CrystEngComm* 15 (17) 2013: pp. 3436 – 3441. https://doi.org/10.1039/C3CE00041A
2. **Cudennec, Y., Lecerf, A.** Topotactic Transformations of Goethite and Lepidocrocite into Hematite and Maghemite *Solid State Sciences* 7 (5) 2005: pp. 520 – 529. http://dx.doi.org/10.1016/j.solidstatesciences.2005.02.002
3. **Yao, Y.Y.** The Oxidation of Hydrocarbons and CO Over Metal Oxides. III. Co_3O_4 *Journal of Catalysis* 33 1974: pp. 108 – 122. https://doi.org/10.1016/0021-9517(74)90250-4
4. **Xie, X., Li, Y., Liu, Z.Q., Haruta, M., Shen, W.** Low-temperature Oxidation of CO Catalysed by Co_3O_4 Nanorods *Nature* 458 (7239) 2009: pp. 746 – 749. https://doi.org/10.1038/nature07877
5. **Wang, J., Du, G., Zeng, R., Niu, B., Chen, Z., Guo, Z., Dou, S.** Porous Co_3O_4 Nanoplatelets by Self-supported Formation as Electrode Material for Lithium-ion Batteries *Electrochimica Acta* 55 (16) 2010: pp. 4805 – 4811. https://doi.org/10.1016/j.electacta.2010.03.048
6. **Lou, X.W., Deng, D., Lee, J.Y., Feng, J., Archer, L.A.** Self-Supported Formation of Needlelike Co_3O_4 Nanotubes and Their Application as Lithium-Ion Battery Electrodes *Advanced Materials* 20 (2) 2008: pp. 258 – 262. https://doi.org/10.1002/adma.200702412
7. **Tian, L., Zou, H., Fu, J., Yang, X., Wang, Y., Guo, H., Fu, X., Liang, C., Wu, M., Shen, P.K., Gao, Q.** Topotactic Conversion Route to Mesoporous Quasi-Single-Crystalline Co_3O_4 Nanobelts with Optimizable Electrochemical Performance *Advanced Functional Materials* 20 (4) 2010: pp. 617 – 623. http://doi.org/10.1002/adfm.200901503
8. **Vidotti, M., van Greco, C., Ponzio, E.A., Córdoba de Torresi, S.I.** Sonochemically Synthesized $Ni(OH)_2$ and $Co(OH)_2$ Nanoparticles and Their Application in Electrochromic Electrodes *Electrochemistry Communications* 8 (4) 2006: pp. 554 – 560. http://dx.doi.org/10.1016/j.elecom.2006.01.024
9. **Yeh, Y., Liu, I.H., Shen, P.** Onset Coarsening/Coalescence of Cobalt Oxides in the Form of Nanoplates Versus Equi-axed Micron Particles *Journal of the European Ceramic Society* 30 (3) 2010: pp. 677 – 688. http://doi.org/10.1016/j.jeurceramsoc.2009.09.004
10. **Tian, L., Huang, K., Liu, Y., Liu, S.** Topotactic Synthesis of Co_3O_4 Nanoboxes from $Co(OH)_2$ Nanoflakes *Journal of Solid State Chemistry* 184 (11) 2011: pp. 2961 – 2965. http://dx.doi.org/10.1016/j.jssc.2011.08.026
11. **Deng, D., Xing, X., Chen, N., Li, Y., Wang, Y.** Hydrothermal synthesis of β-$Co(OH)_2$ nanoplatelets: A novel catalyst for CO oxidation *Journal of Physics and Chemistry of Solids* 100 2017: pp. 107 – 114. https://doi.org/10.1016/j.jpcs.2016.09.021
12. **Fernández-Osorio, A., Vázquez-Olmos, A., Sato-Berru, R., Escudero, R.** Hydrothermal Synthesis of Co_3O_4 Nanooctahedra and Their Magnetic Properties *Reviews on advanced Materials Science* 22 2009: pp. 60 – 66. http://www.ipme.ru/e-journals/RAMS/no_12209/fernandez-osorio.html
13. **Du, N., Zhang, H., Chen, B.D., Wu, J.B., Ma, X.Y., Liu, Z.H., Zhang, Y.Q., Yang, D.R., Huang, X.H., Tu, J.P.** Porous Co_3O_4 Nanotubes Derived from $Co_4(CO)_{12}$ Clusters on Carbon Nanotube Templates: A Highly Efficient Material for Li-Battery Applications *Advanced Materials* 19 (24) 2007: pp. 4505 – 4509. http://doi.org/10.1002/adma.200602513
14. **Shim, H.S., Shinde, V.R., Kim, H.J., Sung, Y.E., Kim, W.B.** Porous Cobalt Oxide Thin Films from Low Temperature Solution Phase Synthesis for Electrochromic Electrode *Thin Solid Films* 516 2008: pp. 8573 – 8578. https://doi.org/10.1016/j.tsf.2008.05.055
15. **Wang, Y., Liu, C., Bai, Y., Chen, H., Ji, Y., Lu, X.** Thermal Dynamics of Alkali Aqueous Solution in Hydrothemal Reaction Vessel *Journal of Chemical Industry and Engineering (China)* 57 (8) 2006: pp. 1856 – 1864. https://doi.org/10.1007/s10589-005-3075-y